

On the difference between signal and background of the chiral magnetic effect relative to spectator and participant planes in isobar collisions at $\sqrt{s_{\text{NN}}} = 200$ GeV

Bang-Xiang Chen,^{1,2} Xin-Li Zhao,^{1,2} and Guo-Liang Ma^{1,2,*}

¹*Key Laboratory of Nuclear Physics and Ion-beam Application (MOE),
Institute of Modern Physics, Fudan University, Shanghai 200433, China*

²*Shanghai Research Center for Theoretical Nuclear Physics,
NSFC and Fudan University, Shanghai 200438, China*

The search for the chiral magnetic effect (CME) in relativistic heavy-ion collisions helps us understand the \mathcal{CP} symmetry breaking in strong interactions and the topological nature of the QCD vacuum. Since the background and signal of the CME have different correlations with respect to the spectator and participant planes, a two-plane method has been proposed to extract the fraction of the CME signal inside the CME observable of $\Delta\gamma$ from the experimental measurements relative to the two planes. Using a multiphase transport model with different strengths of the CME, we reexamine the two-plane method in isobar collisions at $\sqrt{s_{\text{NN}}} = 200$ GeV. The ratios of the CME signal and background relative to the two different planes are found to be different, which is inconsistent with the assumptions made in the current experimental measurements. The difference arises from the decorrelation of the chiral magnetic effect relative to spectator and participant planes, which originates from final state interactions. Our finding suggests that the current experimental measurements may overestimate the fraction of the CME signal in the CME observable in relativistic heavy-ion collisions.

I. INTRODUCTION

Relativistic heavy-ion collisions not only produce the quark-gluon plasma with strong collectivity [1–7], but also generate the strongest magnetic field known to man as the spectator protons from the target and the projectile pass through each other almost at the speed of light [8–12]. This provides a unique experimental way to study the topological properties of the QCD vacuum and the anomalous chiral transport phenomena under the strong magnetic field [13–16]. A well-known detection method is by the chiral magnetic effect (CME), which leads to the phenomenon in which the electric charges in a system with a chiral imbalance are separated along the direction of the magnetic field [17–19].

The charge-dependent azimuthal correlation was first proposed as a possible observable to detect the CME [20], i.e., $\gamma_{\alpha\beta} = \langle \cos(\phi_\alpha + \phi_\beta - 2\Psi_{\text{RP}}) \rangle$, where $\phi_{\alpha(\beta)}$ is the azimuthal angle of a charged particle $\alpha(\beta)$, and Ψ_{RP} is the angle of the reaction plane, and $\Delta\gamma$ represents the difference between opposite-charge and same-charge correlations. The first measurements of the charge-dependent azimuthal correlation from the STAR Collaboration [21–24] at RHIC and the ALICE Collaboration [25] at the LHC are consistent with the expectations of the CME. Unfortunately, some significant background effects contribute to the measured correlator due to the strong collective flow, especially from the elliptic flow [26–30]. The recent RHIC-STAR measurements gave a strict constraint that the CME fraction extracted in Au+Au 200 GeV is quite small, less than 10% [31–34]. To distin-

guish the possible CME signal from the dominant background, many different methods or schemes have been proposed [35]. One of the most important schemes is to use isobar collisions because the two isobar systems ($^{96}_{44}\text{Ru} + ^{96}_{44}\text{Ru}$ and $^{96}_{40}\text{Zr} + ^{96}_{40}\text{Zr}$) have a same nucleon number but different proton numbers [36]. It was expected that there could be a 20% difference in the CME signal with similar elliptic-flow induced backgrounds [37–40]. This prompted the RHIC-STAR Collaboration to conduct the isobar collision experiment for $^{96}_{44}\text{Ru} + ^{96}_{44}\text{Ru}$ and $^{96}_{40}\text{Zr} + ^{96}_{40}\text{Zr}$ collisions at $\sqrt{s_{\text{NN}}} = 200$ GeV [41, 42].

Since the CME signal is positively correlated with the strength of the magnetic field, the ratio of the CME signal from Ru+Ru collisions to that Zr+Zr collisions was theoretically predicted to be larger than unity. However, the newly released experimental results by STAR observed the ratios for various CME observables are all smaller than unity [42]. It indicates that the background effects dominate over the CME signal, and the CME signal is either absent or very small in isobar collisions. Interpreting the isobar experimental results has recently become a hot research direction. For example, different nuclear deformations or nuclear structures have been used to explain the differences in multiplicity and harmonic flows between the two isobar systems [43–48]. Considering both the halo-type neutron skin structure and CME-like charge separation, we have demonstrated that it is difficult for the CME observables to distinguish the presence or absence of the CME, if the CME strength is weak in isobar collisions [49]. At the same time, it was found that the STAR results favor a finite CME signal contribution of about $(6.8 \pm 2.6)\%$, based on the recent finding in the AVFD model [50].

Many experimental observables have been used to detect the CME in Au+Au and isobar collisions. A two-plane measurement method that utilizes the charge-

*Electronic address: glima@fudan.edu.cn

dependent azimuthal correlations with respect to the spectator plane (SP) and participant plane (PP) has been proposed in Refs. [51, 52], because the background and the CME signal have different sensitivities or correlations to the two planes [53]. The STAR collaboration has used the method to detect the fraction of the CME signal inside the inclusive $\Delta\gamma$ correlation in both Au+Au and isobar collisions. For Au + Au collision at $\sqrt{s_{NN}} = 200$ GeV, the STAR results show that the fraction of the CME-induced charge separation is consistent with zero in peripheral centrality bins, but possibly finite CME signals exist in mid-central centrality bins [54]. And no obvious CME signal is observed in isobar collisions at $\sqrt{s_{NN}} = 200$ GeV. This method is believed to remove most of the effect of collective flow in the background effect, but some background effect of non-flow needs further study. Regarding its methodology, it is assumed that the ratio a of elliptic flow with respect to different reaction planes is as same as the ratio b of CME signals with respect to different reaction planes. However, it is possible that the two ratios are different. The assumption of equivalence in the current measurements is due to the lack of theoretical studies on the ratio b [54–56]. This open question makes our current interpretation of the experimental results somewhat questionable. To solve the problem, it is essential to theoretically study the ratio between the CME signals with respect to different reaction planes. This prompted us to calculate the ratios of a and b in isobar collisions at $\sqrt{s_{NN}} = 200$ GeV by using a multiphase transport (AMPT) model with an initial CME signal, in order to provide some theoretical support to the experimental measurement of the CME.

The paper is organized as follows. In Sec. II, we introduce the setting up of the AMPT model with an initial CME signal for isobar collisions and our two-plane method to extract the fraction of the CME signal to the inclusive $\Delta\gamma$. In Sec. III, we present and compare our model results with the measurements from the STAR experiment, and discuss the impact of our findings on the interpretation of experimental data and the possible physics sources. Finally, a summary is given in Sec. IV.

II. MODEL AND METHOD

A. The AMPT model with initial CME signal

The AMPT model is a hybrid transport model with four software packages to simulate four main stages in relativistic heavy-ion collisions [57–59]: (1) The HIJING model provides the initial condition. The transverse density profile of the colliding nucleus is taken to as a Woods-Saxon distribution. The multiple scatterings among participant nucleons produce the spatial and momentum distributions of minijet partons and soft excited strings. With a string melting mechanism, the quark plasma is produced by melting the parent hadrons. (2) Zhang’s parton cascade model is used to simulate the stage of

parton cascade. The ZPC model describes parton interactions with two-body elastic scatterings. The parton cross section is calculated by the leading-order pQCD for gluon-gluon interaction. (3) A quark coalescence model combines two or three nearest partons into hadrons to mimic the hadronization. (4) A relativistic transport (ART) model simulates the stage of hadronic rescatterings, including both resonance decays and all hadronic reactions for elastic and inelastic scatterings for baryon-baryon, baryon-meson, and meson-meson interactions. Many previous studies have shown that the AMPT model can describe well the various experimental observables in both large and small colliding systems at RHIC and the LHC [57–66].

To simulate isobar collisions, the spatial distributions of nucleons inside $^{96}_{44}\text{Ru}$ and $^{96}_{40}\text{Zr}$ in the rest frame are sampled according to the Woods-Saxon form in spherical coordinates,

$$\rho(r, \theta) = \rho_0 / \{1 + \exp[(r - R(\theta, \phi))/a_0]\}, \quad (1)$$

$$R(\theta, \phi) = R_0[1 + \beta_2 Y_{2,0}(\theta, \phi) + \beta_3 Y_{3,0}(\theta, \phi)], \quad (2)$$

in which ρ_0 is the normal nuclear density, a_0 is the surface diffuseness parameter, R_0 is the nucleus radius, and β_2 and β_3 are the quadrupole and octupole deformities for the nucleus. In our previous work [49], we found that the halo-type neutron skin case is the best one among the eighteen cases which can describe the experimental ratios of charged-particle multiplicity distribution, the average number of charged particles, and elliptic flow. Therefore, we also choose the halo-type neutron skin case in this study, where no deformation for both $^{96}_{44}\text{Ru}$ and $^{96}_{40}\text{Zr}$ ($\beta_2 = \beta_3 = 0$), $R_0 = 5.085$ and $a_0 = 0.523$ for both protons and neutrons inside $^{96}_{44}\text{Ru}$, but $R_0 = 5.021$ and $a_0 = 0.523$ for protons and $R_0 = 5.021$ and $a_0 = 0.592$ for neutrons inside $^{96}_{40}\text{Zr}$ due to the possible existence of neutron halo for $^{96}_{40}\text{Zr}$.

A CME-like charge separation has been introduced into the initial partonic stage of the AMPT model in Ref. [67]. By tuning the percentage p , which defines what percentage of quarks join the charge separation, we can control the signal strength of the CME. The definition of p is

$$p = \frac{N_{\uparrow(\downarrow)}^{+(-)} - N_{\downarrow(\uparrow)}^{+(-)}}{N_{\uparrow(\downarrow)}^{+(-)} + N_{\downarrow(\uparrow)}^{+(-)}}, \quad (3)$$

where N is the number of quarks of a given species (u or d or s), $+$ and $-$ denote positive and negative charges of quarks, and \uparrow and \downarrow represent the moving directions of quarks along the magnetic field. Considering that the magnetic fields for Ru + Ru and Zr + Zr collisions are different [53], we practically make the initial charge separation based on the magnitude and direction of the magnetic field by calculating the magnetic field for each event. We denote p as the CME strength in Ru+Ru collisions, for example, $p = 2\%$ means $p_{\text{Ru+Ru}} = 2\%$ and $p_{\text{Zr+Zr}} = 2\%/1.15 = 1.74\%$ since we keep $p_{\text{Ru+Ru}}/p_{\text{Zr+Zr}} = 1.15$.

B. Spectator and participant planes

In the two-plane method, the elliptic flow-driven background is believed to be more relevant to the participant plane (PP), but the CME signal is more relevant to the spectator plane (SP) [51, 52]. We reconstruct the spectator and participant planes by using the two following equations, respectively,

$$\psi_{\text{SP}} = \frac{\text{atan} 2 (\langle r_n^2 \sin(2\phi_n) \rangle, \langle r_n^2 \cos(2\phi_n) \rangle)}{2}, \quad (4)$$

$$\psi_{\text{PP}} = \frac{\text{atan} 2 (\langle r_p^2 \sin(2\phi_p) \rangle, \langle r_p^2 \cos(2\phi_p) \rangle) + \pi}{2}, \quad (5)$$

where r_n and ϕ_n are the displacement and azimuthal angle of spectator neutrons in the transverse plane, respectively, and r_p and ϕ_p are the displacement and azimuthal angle of participating partons in the transverse plane, respectively. All spatial information about the displacement and azimuthal angle is obtained from the initial state of the AMPT model. With the two different planes, the corresponding elliptic flow, $v_2\{\text{SP}\}$ and $v_2\{\text{PP}\}$, can be calculated as follows, respectively,

$$v_2\{\text{SP}\} = \langle \cos 2(\phi - \psi_{\text{SP}}) \rangle, \quad (6)$$

$$v_2\{\text{PP}\} = \langle \cos 2(\phi - \psi_{\text{PP}}) \rangle. \quad (7)$$

The upper panel in Fig. 1 shows the centrality dependence of $v_2\{\text{PP}\}$ and $v_2\{\text{SP}\}$ of charged hadrons from the AMPT model with different strengths of the CME in Ru + Ru and Zr + Zr collisions at $\sqrt{s_{\text{NN}}} = 200$ GeV. We can see that $v_2\{\text{PP}\}$ is greater than $v_2\{\text{SP}\}$ for all cases, since elliptic flow is more correlated to the participant plane than the spectator plane. On the other hand, for the central and mid-central centrality of 0–50%, both $v_2\{\text{PP}\}$ and $v_2\{\text{SP}\}$ decrease slightly with increasing CME signal strength. For the peripheral centrality of 50–80%, both $v_2\{\text{PP}\}$ and $v_2\{\text{SP}\}$ are insensitive to the strength of CME signal. The lower panel in Fig. 1 shows the $v_2\{\text{PP}\}$ and $v_2\{\text{SP}\}$ ratios of Ru + Ru to Zr + Zr. The ratio of $v_2\{\text{SP}\}$ is greater than that of $v_2\{\text{PP}\}$. The trend in the ratio results has been found to be caused by the nuclear structures of Ru and Zr [49].

C. Two-plane method to extract f_{cme}

In this subsection, the two-plane method for detecting the CME signal is introduced first, and then how to improve the two-plane method using the AMPT model is discussed. The experimentally measured CME observable $\Delta\gamma$ includes the CME signal and the background effect mainly arising from the contributions of elliptical flow and non-flow effects. Therefore, the experimentally

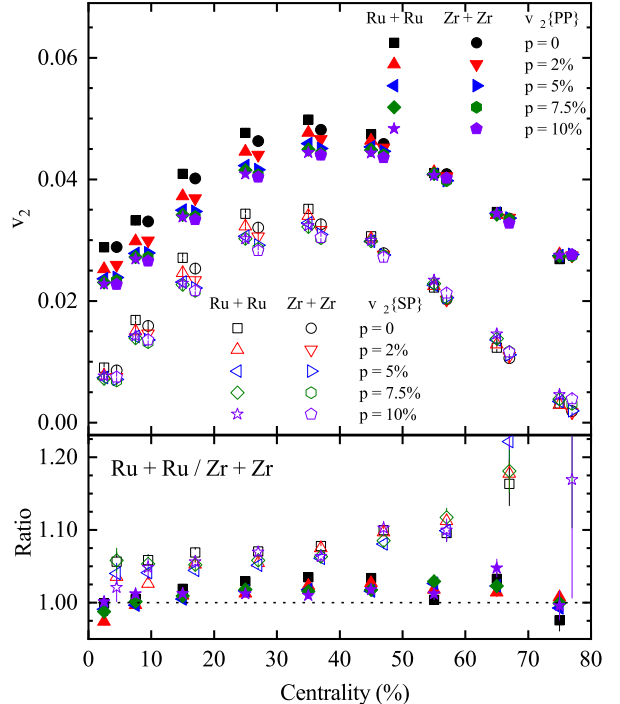


FIG. 1: (Color online) Upper panel: AMPT results on centrality dependences of elliptic flow $v_2\{\text{PP}\}$ (solid symbols) and $v_2\{\text{SP}\}$ (open symbols) in isobar collisions at $\sqrt{s_{\text{NN}}} = 200$ GeV from the AMPT model with different strengths of the CME. Lower panel: AMPT results on $v_2\{\text{PP}\}$ and $v_2\{\text{SP}\}$ ratios of Ru + Ru collisions to Zr + Zr collisions as a function of centrality bin.

measured CME observable $\Delta\gamma$ with respect to different planes can be divided into two parts as follows,

$$\Delta\gamma\{\psi\} = \Delta\gamma_{\text{Bkg}}\{\psi\} + \Delta\gamma_{\text{CME}}\{\psi\} \quad (8)$$

where ψ can represent ψ_{PP} or ψ_{SP} . The ratios of the elliptic flow and the measured observable with two different planes can be defined by a and A as follows, respectively,

$$a = v_2\{\text{SP}\}/v_2\{\text{PP}\}, \quad (9)$$

$$A = \Delta\gamma\{\text{SP}\}/\Delta\gamma\{\text{PP}\}. \quad (10)$$

Since the CME signal can not be measured directly in an experiment, people usually assume that the ratio of the CME signals of different reaction planes is the inverse of a . Thus, the following relation can be obtained,

$$\Delta\gamma\{\text{SP}\} = a\Delta\gamma_{\text{Bkg}}\{\text{PP}\} + \Delta\gamma_{\text{CME}}\{\text{PP}\}/a. \quad (11)$$

After a simple transformation, the percentage of the CME signal inside the measured CME observable (f_{CME}) is obtained by,

$$f_{\text{CME}} = \frac{\Delta\gamma_{\text{CME}}\{\text{PP}\}}{\Delta\gamma\{\text{PP}\}} = \frac{A/a - 1}{1/a^2 - 1}. \quad (12)$$

Equation (12) indicates that the percentage of the CME signal inside the measured CME observable can be obtained by measuring A and a . However, it has been pointed out in Refs. [55, 56] that the ratio of the CME signal and the inverse ratio of the elliptic flow could be different. Let us assume the following relation holds,

$$\Delta\gamma_{\text{CME}}\{\text{PP}\} = b\Delta\gamma_{\text{CME}}\{\text{SP}\}. \quad (13)$$

where b represents the ratio of the CME signals with respect to different planes. By replacing the corresponding part in Eq. (11), a more realistic relation can be obtained as shown below,

$$\Delta\gamma\{\text{SP}\} = a\Delta\gamma_{\text{Bkg}}\{\text{PP}\} + \Delta\gamma_{\text{CME}}\{\text{PP}\}/b. \quad (14)$$

Thus, the more realistic percentage of the CME signal inside the measured CME observable should be calculated by,

$$f_{\text{CME}}\{b\} = \frac{\Delta\gamma_{\text{CME}}\{\text{PP}\}}{\Delta\gamma\{\text{PP}\}} = \frac{A/a - 1}{1/ab - 1}, \quad (15)$$

after considering b .

The left task is calculating b , which can be done theoretically. In the AMPT model, the CME signal is simulated by affecting a certain proportion of partons at the initial state. The proportion of CME particles is denoted by p in this paper. Within our theoretical framework, the value of b can be obtained by using the following equation,

$$b = \frac{\Delta\gamma\{\text{PP}\}(p \neq 0) - \Delta\gamma\{\text{PP}\}(p = 0)}{\Delta\gamma\{\text{SP}\}(p \neq 0) - \Delta\gamma\{\text{SP}\}(p = 0)}, \quad (16)$$

where the numerator and denominator are the CME signal inside the measured CME observable with respect to participant and spectator planes, respectively.

III. RESULTS AND DISCUSSIONS

In this section, we present the AMPT results on charge-dependent azimuthal correlations for charged particles relative to spectator and participant planes, and compare them with the results of the STAR isobar experiment. Our kinetic cuts are $0.2 < p_T < 2.0$ GeV/ c and $|\eta| < 1$, as same as the STAR experiment.

The upper panel in Fig. 2 shows the centrality dependence of $\Delta\gamma\{\text{PP}\}$ and $\Delta\gamma\{\text{SP}\}$ from the AMPT model with different strengths of the CME in Ru + Ru and Zr + Zr collisions at $\sqrt{s_{\text{NN}}} = 200$ GeV. Compared to

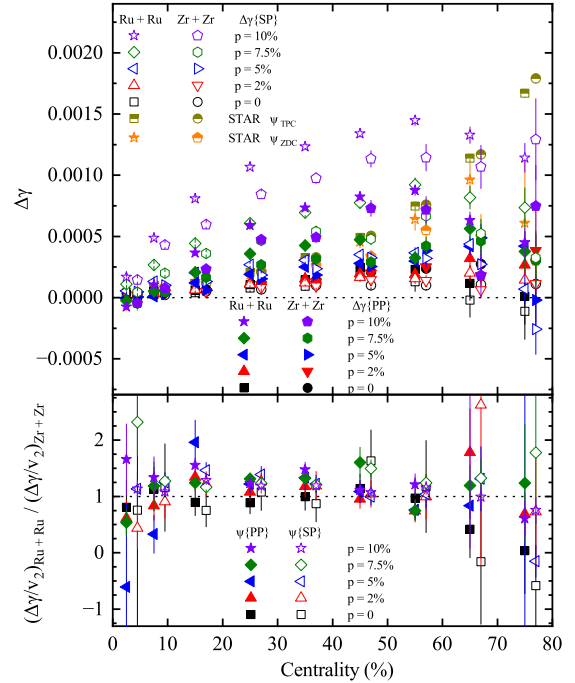


FIG. 2: (Color online) Upper panel: The centrality dependences of $\Delta\gamma\{\text{PP}\}$ (solid symbols) and $\Delta\gamma\{\text{SP}\}$ (open symbols) in isobar collisions at $\sqrt{s_{\text{NN}}} = 200$ GeV from the AMPT model with different strengths of the CME, in comparison with the STAR data [42]. Lower panel: The centrality dependences of $\Delta\gamma/v_2$ ratios of Ru + Ru collisions to Zr + Zr collisions. The data points are shifted along the x axis for clarity.

the STAR data, a small percentage of CME signal is preferred, which is also consistent with our recent study [49]. The $\Delta\gamma\{\text{SP}\}$ is greater than $\Delta\gamma\{\text{PP}\}$, which indicates that $\Delta\gamma\{\text{SP}\}$ is more sensitive to the CME than $\Delta\gamma\{\text{PP}\}$ since the spectator plane is more strongly correlated to the direction of the magnetic field than the participant plane. The lower panel in Fig. 2 shows the $\Delta\gamma/v_2$ ratios of Ru + Ru to Zr + Zr. Within our statistical errors, the ratios are consistent with unity.

Figure 3 shows the centrality dependences of $A = \Delta\gamma\{\text{SP}\}/\Delta\gamma\{\text{PP}\}$ and $a = v_2\{\text{SP}\}/v_2\{\text{PP}\}$ from the AMPT model with different strengths of the CME, compared with the STAR experimental data [42]. As the CME strength in the AMPT model increases, the value of a hardly changes and is always less than unity. It indicates that the CME has the same impact on v_2 with respect to different planes. For $p=0$ and $p=2\%$, the values of A are almost identical and smaller than unity. However, in the other cases, it is greater than unity and increases with increasing p . This indicates that the CME has different effects on $\Delta\gamma$ relative to different planes.

Figure 4 shows the A/a ratio as a function of centrality given by the AMPT model for different strengths of the

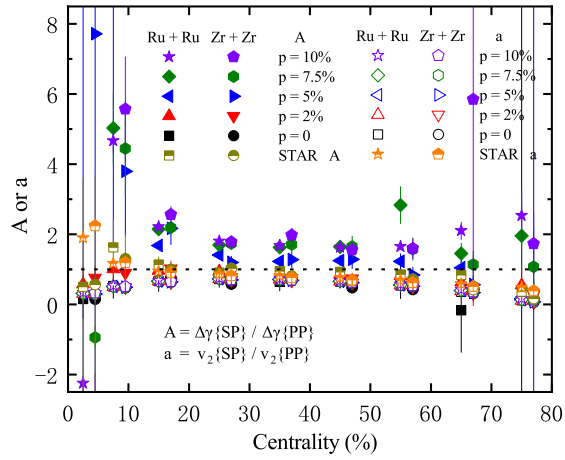


FIG. 3: (Color online) The centrality dependences of A and a in isobar collisions at $\sqrt{s_{NN}} = 200$ GeV from the AMPT model with different strengths of the CME, in comparison with the STAR data [42]. The solid and open symbols represent the results for A and a , respectively. The data points are shifted along the x axis for clarity.

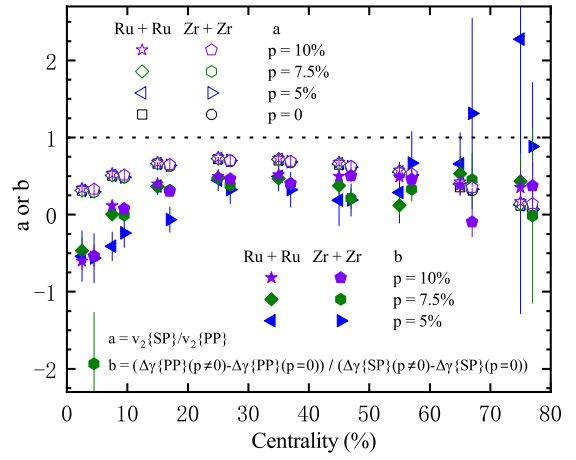


FIG. 5: (Color online) The centrality dependences of a and b in isobar collisions at $\sqrt{s_{NN}} = 200$ GeV from the AMPT model with different strengths of the CME. The open and solid symbols represent the results for a and b , respectively. The data points are shifted along the x axis for clarity.

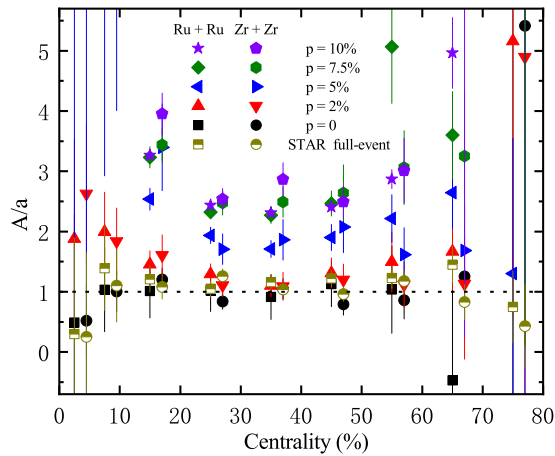


FIG. 4: (Color online) The centrality dependences of A/a in isobar collisions at $\sqrt{s_{NN}} = 200$ GeV from the AMPT model with different strengths of the CME, in comparison with the STAR data [42]. The data points are shifted along the x axis for clarity.

CME. From Eq. (12) or Eq. (15), the value of $A/a > 1$ corresponds to the presence of a CME signal inside the CME observable $\Delta\gamma$. Let us focus on mid-central collisions where the CME effect is expected to be more likely to be measured than at the other centrality bins. For the 20-50% centrality bin, we can see $A/a > 1$ clearly except the cases of $p=0$ and $p=2\%$. Moreover, we observe that the value of A/a increases as the CME strength increases. It indicates that A/a can reflect the strength of the CME signal.

We calculate b using Eq. (16) and compare it with a . Figure 5 shows the centrality dependence of a and b from the AMPT model with different strengths of the CME.

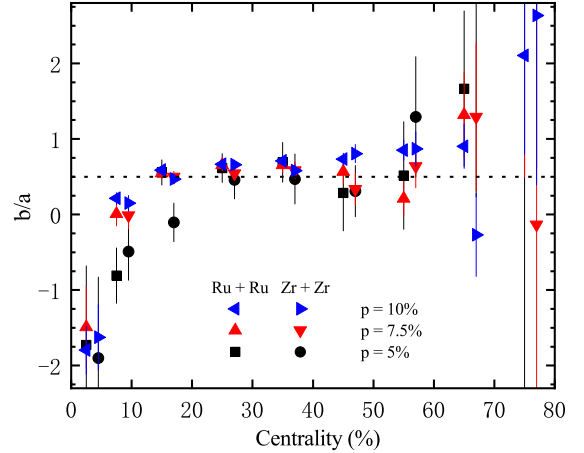


FIG. 6: (Color online) The centrality dependences of b/a in isobar collisions at $\sqrt{s_{NN}} = 200$ GeV from the AMPT model with different strengths of the CME. The data points are shifted along the x axis for clarity.

We find that the values of a and b are different. The value of b is smaller than the value of a at the 20-50% centrality bin. The value of a is almost independent of the CME strength, as same as shown in Fig. 3. Considering statistical errors, the value of b does not vary significantly with the CME strengths. Note that the case of the 2% CME strength is not shown due to huge statistical errors.

Figure 6 further shows the centrality dependence of the b/a ratio from the AMPT model with different strengths of the CME. For the 20-50% centrality bin in isobar collisions at $\sqrt{s_{NN}} = 200$ GeV, such an approximate relation that $b = a/2$ can be obtained by a constant function fitting. It implies that the relative ratio of the CME signals with respect to different planes is not equal to the inverse

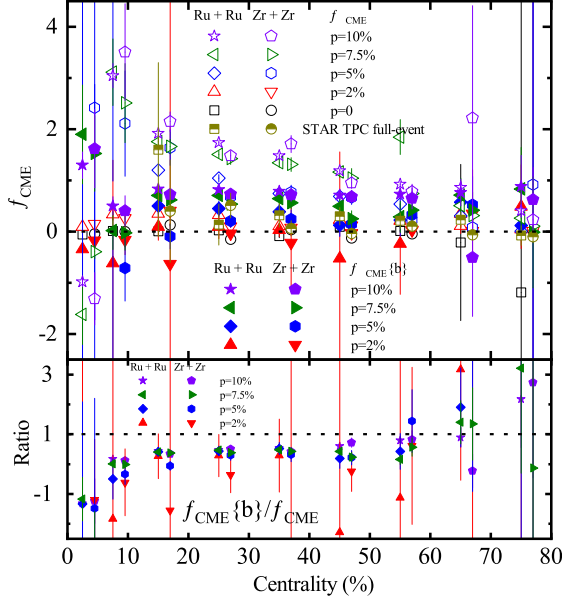


FIG. 7: (Color online) Upper panel: The centrality dependences of $f_{\text{CME}}\{b\}$ and f_{CME} in isobar collisions at $\sqrt{s_{\text{NN}}} = 200$ GeV from the AMPT model with different strengths of the CME, in comparison with the STAR data [42]. The solid and open symbols represent the results for $f_{\text{CME}}\{b\}$ and f_{CME} , respectively. Lower panel: The centrality dependences of the ratio of $f_{\text{CME}}\{b\}$ to f_{CME} . The data points are shifted along the x axis for clarity.

of the elliptic flow ratio with respect to different planes. Next, we will show that this finding has important implications for extracting the fraction of the CME signal inside the $\Delta\gamma$ observable.

The upper panel in Fig. 7 shows two kinds of f_{CME} as a function of centrality from the AMPT model with different strengths of the CME, where the solid and open symbols represent f_{CME} calculated from Eq. (12) and $f_{\text{CME}}\{b\}$ calculated from Eq. (15), respectively. Compared to the STAR experimental data [42], the results of f_{CME} from $p=0\%$ or $p=2\%$ are favored. For the 20-50% centrality bin, when p is not equal to zero, $f_{\text{CME}}\{b\}$ is found to be less than f_{CME} . The lower panel in Fig. 7 shows the centrality dependence of the ratio of $f_{\text{CME}}\{b\}$ to f_{CME} . For the 20-50% centrality bin, the ratio is less than unity. It indicates that the fraction of the CME signal inside the $\Delta\gamma$ observable will be overestimated if assuming $b = a$.

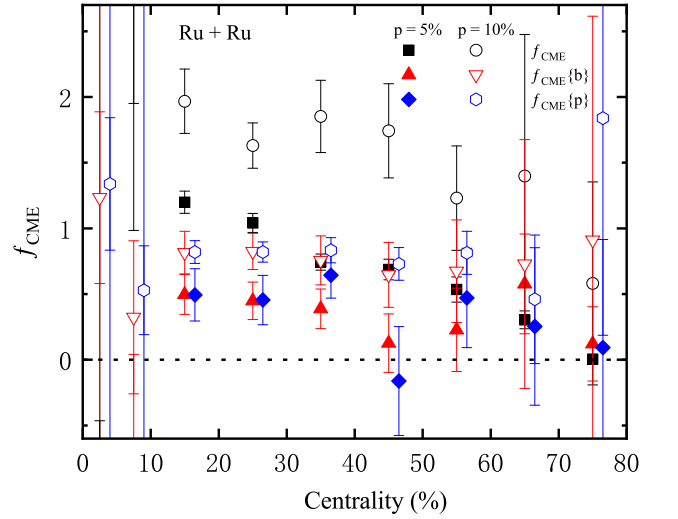


FIG. 8: (Color online) The centrality dependences of f_{CME} , $f_{\text{CME}}\{b\}$ and $f_{\text{CME}}\{p\}$ from three different methods in Ru + Ru collisions at $\sqrt{s_{\text{NN}}} = 200$ GeV from the AMPT model with two different strengths of the CME. The data points are shifted along the x axis for clarity.

To discern which of these two above f_{CME} is closer to the real situation, we can theoretically use another method to obtain the true f_{CME} , namely $f_{\text{CME}}\{p\}$, as defined as follows,

$$f_{\text{CME}}\{p\} = \frac{\Delta\gamma_{\text{CME}}\{\text{PP}\}(p \neq 0)}{\Delta\gamma\{\text{PP}\}(p \neq 0)}, \quad (17)$$

where

$$\Delta\gamma_{\text{CME}}\{\text{PP}\}(p \neq 0) = \Delta\gamma\{\text{PP}\}(p \neq 0) - \Delta\gamma\{\text{PP}\}(p = 0). \quad (18)$$

The observables of $\Delta\gamma\{\text{PP}\}(p = 0)$ and $\Delta\gamma\{\text{PP}\}(p \neq 0)$ can be obtained from the AMPT model without the CME and with different strengths of the CME, respectively. In Fig. 8, compared to the true f_{CME} , we find that $f_{\text{CME}}\{b\}$ is closer to and consistent with $f_{\text{CME}}\{p\}$ than f_{CME} for the 10–50% centrality bin. This suggests that it is necessary to consider b to obtain a more reliable f_{CME} .

From the above results, it is clear that $b = a/2$ significantly impacts the final result of f_{CME} in isobar collisions. To understand where this relation comes from, we calculate a and b for different stages in Ru + Ru collision at $\sqrt{s_{\text{NN}}} = 200$ GeV in the AMPT model with the CME strength of $p = 10\%$. We focus on four evolution stages of heavy-ion collisions: the initial stage, after parton cascade, after coalescence, and after hadron rescatterings. In the upper panel of Fig. 9, we can find that the value of a remains constant for the last three stages. Note that we do not show a for the initial stage, since the elliptic flow is initially zero. However, the value of b is always smaller than that of a and decreases stage by stage for the 10-50% centrality bin. In the lower panel of Fig. 9, the ratio of b/a also decreases with the stage evolution. The

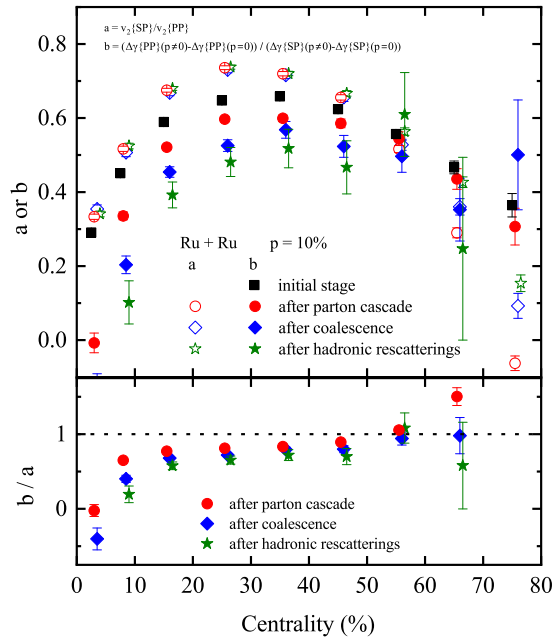


FIG. 9: (Color online) Upper panel: The centrality dependences of a and b in Ru + Ru collisions at $\sqrt{s_{\text{NN}}} = 200$ GeV for four different stages from the AMPT model with the CME strength of $p = 10\%$. The open and solid symbols represent the results for a and b , respectively. Lower panel: The centrality dependences of the ratio of b/a for the different stages in Ru + Ru collisions. The data points are shifted along the x axis for clarity.

main reason is due to the change in b . The decreasing of b indicates the correlation between the CME signals relative to different planes becomes less and less correlated, which can be understood as a consequence of the decorrelation resulting from final state interactions during the evolution of heavy-ion collisions [49, 67, 68].

IV. SUMMARY

Using a multiphase transport model with different strengths of the CME, we reexamine the proposed two-

plane method to determine the fraction of the CME signal inside the CME observable of $\Delta\gamma$ in isobar collisions at $\sqrt{s_{\text{NN}}} = 200$ GeV. We first calculate the elliptic flow v_2 and the CME observable of $\Delta\gamma$ with respect to the spectator plane and participant plane. The ratio b of the CME signal relative to the two different planes is found to be different from the ratio a of background relative to the two different planes in isobar collisions. If the difference between a and b is taken into account, we demonstrate that it will lead to a smaller CME fraction than the constraint obtained in current experimental way. We theoretically observe a decrease in the value of b during the stage evolution in the AMPT model, which indicates the decorrelation of the chiral magnetic effect relative to spectator and participant planes is caused by final state interactions in isobar collisions. Since a and b were assumed to be equal in the current experimental study, the fraction of the CME signal could be overestimated. We hope that our study will provide a theoretical reference for future accurate measurements of the fraction of the chiral magnetic effect inside the experimental observable in relativistic heavy-ion collisions.

ACKNOWLEDGMENTS

We thank Prof. Jie Zhao for the helpful discussions. This work is supported by the National Natural Science Foundation of China under Grants No.12147101, No. 11890714, No. 11835002, No. 11961131011, No. 11421505, No. 12105054, the National Key Research and Development Program of China under Grant No. 2022YFA1604900, the Strategic Priority Research Program of Chinese Academy of Sciences under Grant No. XDB34030000, and the Guangdong Major Project of Basic and Applied Basic Research under Grant No. 2020B0301030008.

-
- [1] P. F. Kolb, J. Sollfrank, and U. W. Heinz, Phys. Rev. C **62**, 054909 (2000), hep-ph/0006129.
 - [2] D. Teaney, J. Lauret, and E. V. Shuryak, Phys. Rev. Lett. **86**, 4783 (2001), nucl-th/0011058.
 - [3] L. Yan, Chin. Phys. C **42**, 042001 (2018), 1712.04580.
 - [4] C. Shen and L. Yan, Nucl. Sci. Tech. **31**, 122 (2020), 2010.12377.
 - [5] H. Song, Y. Zhou, and K. Gajdosova, Nucl. Sci. Tech. **28**, 99 (2017), 1703.00670.
 - [6] S.-W. Lan and S.-S. Shi, Nucl. Sci. Tech. **33**, 21 (2022).
 - [7] S. Wu, C. Shen, and H. Song, Chin. Phys. Lett. **38**, 081201 (2021), 2104.13250.
 - [8] V. Skokov, A. Y. Illarionov, and V. Toneev, Int. J. Mod. Phys. A **24**, 5925 (2009), 0907.1396.
 - [9] A. Bzdak and V. Skokov, Phys. Lett. B **710**, 171 (2012), 1111.1949.
 - [10] W.-T. Deng and X.-G. Huang, Phys. Rev. C **85**, 044907 (2012), 1201.5108.
 - [11] X.-L. Zhao, Y.-G. Ma, and G.-L. Ma, Phys. Rev. C **97**, 024910 (2018), 1709.05962.
 - [12] X.-L. Zhao, G.-L. Ma, and Y.-G. Ma, Phys. Lett. B **792**, 413 (2019), 1901.04156.

- [13] D. E. Kharzeev and J. Liao, *Nature Rev. Phys.* **3**, 55 (2021), 2102.06623.
- [14] X.-G. Huang, *Rept. Prog. Phys.* **79**, 076302 (2016), 1509.04073.
- [15] K. Hattori and X.-G. Huang, *Nucl. Sci. Tech.* **28**, 26 (2017), 1609.00747.
- [16] J.-H. Gao, G.-L. Ma, S. Pu, and Q. Wang, *Nucl. Sci. Tech.* **31**, 90 (2020), 2005.10432.
- [17] D. Kharzeev, *Phys. Lett. B* **633**, 260 (2006), hep-ph/0406125.
- [18] D. E. Kharzeev, L. D. McLerran, and H. J. Warringa, *Nucl. Phys. A* **803**, 227 (2008), 0711.0950.
- [19] K. Fukushima, D. E. Kharzeev, and H. J. Warringa, *Phys. Rev. D* **78**, 074033 (2008), 0808.3382.
- [20] S. A. Voloshin, *Phys. Rev. C* **70**, 057901 (2004), hep-ph/0406311.
- [21] B. I. Abelev et al. (STAR), *Phys. Rev. Lett.* **103**, 251601 (2009), 0909.1739.
- [22] B. I. Abelev et al. (STAR), *Phys. Rev. C* **81**, 054908 (2010), 0909.1717.
- [23] L. Adamczyk et al. (STAR), *Phys. Rev. C* **88**, 064911 (2013), 1302.3802.
- [24] L. Adamczyk et al. (STAR), *Phys. Rev. Lett.* **113**, 052302 (2014), 1404.1433.
- [25] B. Abelev et al. (ALICE), *Phys. Rev. Lett.* **110**, 012301 (2013), 1207.0900.
- [26] A. Bzdak, V. Koch, and J. Liao, *Phys. Rev. C* **83**, 014905 (2011), 1008.4919.
- [27] J. Liao, V. Koch, and A. Bzdak, *Phys. Rev. C* **82**, 054902 (2010), 1005.5380.
- [28] S. Schlichting and S. Pratt, *Phys. Rev. C* **83**, 014913 (2011), 1009.4283.
- [29] F. Wang, *Phys. Rev. C* **81**, 064902 (2010), 0911.1482.
- [30] W.-Y. Wu et al. (2022), 2211.15446.
- [31] F.-Q. Wang and J. Zhao, *Nucl. Sci. Tech.* **29**, 179 (2018).
- [32] J. Zhao (STAR), *Nucl. Phys. A* **1005**, 121766 (2021), 2002.09410.
- [33] J. Zhao and F. Wang, *Prog. Part. Nucl. Phys.* **107**, 200 (2019), 1906.11413.
- [34] F. Wang, in *29th International Conference on Ultra-relativistic Nucleus-Nucleus Collisions* (2022), 2207.10044.
- [35] W. Li and G. Wang, *Ann. Rev. Nucl. Part. Sci.* **70**, 293 (2020), 2002.10397.
- [36] S. A. Voloshin, *Phys. Rev. Lett.* **105**, 172301 (2010), 1006.1020.
- [37] W.-T. Deng, X.-G. Huang, G.-L. Ma, and G. Wang, *Phys. Rev. C* **94**, 041901 (2016), 1607.04697.
- [38] V. Koch, S. Schlichting, V. Skokov, P. Sorensen, J. Thomas, S. Voloshin, G. Wang, and H.-U. Yee, *Chin. Phys. C* **41**, 072001 (2017), 1608.00982.
- [39] W.-T. Deng, X.-G. Huang, G.-L. Ma, and G. Wang, *Phys. Rev. C* **97**, 044901 (2018), 1802.02292.
- [40] S. Choudhury et al., *Chin. Phys. C* **46**, 014101 (2022), 2105.06044.
- [41] J. Adam et al. (STAR), *Nucl. Sci. Tech.* **32**, 48 (2021), 1911.00596.
- [42] M. Abdallah et al. (STAR), *Phys. Rev. C* **105**, 014901 (2022), 2109.00131.
- [43] H.-j. Xu, H. Li, X. Wang, C. Shen, and F. Wang, *Phys. Lett. B* **819**, 136453 (2021), 2103.05595.
- [44] H.-j. Xu, W. Zhao, H. Li, Y. Zhou, L.-W. Chen, and F. Wang (2021), 2111.14812.
- [45] C. Zhang and J. Jia, *Phys. Rev. Lett.* **128**, 022301 (2022), 2109.01631.
- [46] J. Jia and C.-J. Zhang (2021), 2111.15559.
- [47] J. Jia, *Phys. Rev. C* **105**, 014905 (2022), 2106.08768.
- [48] J. Jia, *Phys. Rev. C* **105**, 044905 (2022), 2109.00604.
- [49] X.-L. Zhao and G.-L. Ma, *Phys. Rev. C* **106**, 034909 (2022), 2203.15214.
- [50] D. E. Kharzeev, J. Liao, and S. Shi, *Phys. Rev. C* **106**, L051903 (2022), 2205.00120.
- [51] H.-j. Xu, J. Zhao, X. Wang, H. Li, Z.-W. Lin, C. Shen, and F. Wang, *Chin. Phys. C* **42**, 084103 (2018), 1710.07265.
- [52] H.-J. Xu, X. Wang, H. Li, J. Zhao, Z.-W. Lin, C. Shen, and F. Wang, *Phys. Rev. Lett.* **121**, 022301 (2018), 1710.03086.
- [53] X.-L. Zhao, G.-L. Ma, and Y.-G. Ma, *Phys. Rev. C* **99**, 034903 (2019), 1901.04151.
- [54] M. S. Abdallah et al. (STAR), *Phys. Rev. Lett.* **128**, 092301 (2022), 2106.09243.
- [55] S. Shi, Y. Jiang, E. Lilleskov, and J. Liao, *Annals Phys.* **394**, 50 (2018), 1711.02496.
- [56] Y. Feng, J. Zhao, H. Li, H.-j. Xu, and F. Wang, *Phys. Rev. C* **105**, 024913 (2022), 2106.15595.
- [57] Z.-W. Lin, C. M. Ko, B.-A. Li, B. Zhang, and S. Pal, *Phys. Rev. C* **72**, 064901 (2005), nucl-th/0411110.
- [58] G.-L. Ma and Z.-W. Lin, *Phys. Rev. C* **93**, 054911 (2016), 1601.08160.
- [59] Z.-W. Lin and L. Zheng, *Nucl. Sci. Tech.* **32**, 113 (2021), 2110.02989.
- [60] Z.-W. Lin, *Phys. Rev. C* **90**, 014904 (2014), 1403.6321.
- [61] J. D. Orjuela Koop, A. Adare, D. McGlinchey, and J. L. Nagle, *Phys. Rev. C* **92**, 054903 (2015), 1501.06880.
- [62] G.-L. Ma and A. Bzdak, *Nucl. Phys. A* **956**, 745 (2016).
- [63] Y. He and Z.-W. Lin, *Phys. Rev. C* **96**, 014910 (2017), 1703.02673.
- [64] L. Huang and G.-L. Ma, *Chin. Phys. C* **45**, 074110 (2021), 2107.09264.
- [65] Q. Chen and G.-L. Ma, *Phys. Rev. C* **106**, 014907 (2022), 2207.11736.
- [66] Q. Chen, H.-S. Wang, and G.-L. Ma (2022), 2210.17125.
- [67] G.-L. Ma and B. Zhang, *Phys. Lett. B* **700**, 39 (2011), 1101.1701.
- [68] L. Huang, M.-W. Nie, and G.-L. Ma, *Phys. Rev. C* **101**, 024916 (2020), 1906.11631.